crystals

MDPI

Article

Crystallographic Characterization of Sodium Ions in a Bacterial Leucine/Sodium Symporter

Akira Karasawa [1,*], Haijiao Liu [2], Matthias Quick [3,4], Wayne A. Hendrickson [1,4,5] and Qun Liu [2,6,*]

1 Center on Membrane Protein Production and Analysis, New York Structural Biology Center, New York, NY 10027, USA
2 Department of Materials Science and Chemical Engineering, Stony Brook University, Stony Brook, NY 11794, USA
3 Department of Psychiatry, Columbia University Vagelos College of Physicians & Surgeons and New York State Psychiatric Institute, Area Neuroscience—Division of Molecular Therapeutics, New York, NY 10032, USA
4 Department of Physiology and Cellular Biophysics, Columbia University Vagelos College of Physicians & Surgeons, New York, NY 10032, USA
5 Department of Biochemistry and Molecular Biophysics, Columbia University Vagelos College of Physicians & Surgeons, New York, NY 10032, USA
6 Brookhaven National Laboratory, Biology Department, Upton, NY 11973, USA
* Correspondence: akarasawa@nysbc.org (A.K.); qunliu@bnl.gov (Q.L.)

Abstract: Na^+ is the most abundant ion in living organisms and plays essential roles in regulating nutrient uptake, muscle contraction, and neurotransmission. The identification of Na^+ in protein structures is crucial for gaining a deeper understanding of protein function in a physiological context. LeuT, a bacterial homolog of the neurotransmitter:sodium symporter family, uses the Na^+ gradient to power the uptake of amino acids into cells and has been used as a paradigm for the study of Na^+-dependent transport systems. We have devised a low-energy multi-crystal approach for characterizing low-Z ($Z \leq 20$) anomalous scattering ions such as Na^+, Mg^{2+}, K^+, and Ca^{2+} by combining Bijvoet-difference Fourier syntheses for ion detection and f″ refinements for ion speciation. Using the approach, we experimentally identify two Na^+ bound near the central leucine binding site in LeuT. Using LeuT microcrystals, we also demonstrate that Na^+ may be depleted to study conformational changes in the LeuT transport cycle.

Keywords: amino acid transporter; anomalous diffraction; element identification; multiple crystals

check for updates

Citation: Karasawa, A.; Liu, H.; Quick, M.; Hendrickson, W.A.; Liu, Q. Crystallographic Characterization of Sodium Ions in a Bacterial Leucine/Sodium Symporter. *Crystals* **2023**, *13*, 183. https://doi.org/10.3390/cryst13020183

Academic Editor: Abel Moreno

Received: 31 December 2022
Revised: 15 January 2023
Accepted: 16 January 2023
Published: 20 January 2023

Copyright: © 2023 by the authors. Licensee MDPI, Basel, Switzerland. This article is an open access article distributed under the terms and conditions of the Creative Commons Attribution (CC BY) license (https://creativecommons.org/licenses/by/4.0/).

1. Introduction

Na^+ is the most abundant ion in living organisms and plays essential roles in central physiological processes [1]. For example, Na^+ pumps create and maintain an electrochemical gradient of Na^+ across the plasma membrane, and this energy is used for nutrient uptake into cells or neuronal signaling and cardiac muscle contraction [2]. A high concentration of intracellular Na^+ is toxic, and Na^+ is continuously extruded by Na^+ transporters and pumps [3]. Na^+ is also essential for some enzyme activity as a co-factor, for example, β-galactosidase, factor Xa, and thrombin [4]. Therefore, the identification of Na^+ and the determination of its precise location in protein structures can provide important clues for understanding the mechanisms of Na^+ transporters, channels, pumps, and Na^+-dependent enzymes.

LeuT, a bacterial orthologue of the human SLC6 family [5] of the neurotransmitter:sodium symporter (NSS) family, is a Na^+-dependent amino acid symporter [6]. The SLC6 family includes transporters for dopamine [2] and serotonin [7] that play essential roles in the reuptake of neurotransmitters involved in synaptic neurotransmission [8]. The dysfunction of SLC6 family transporters is related to various neurological and psychiatric disorders in humans [9]. LeuT has been used as a model transporter to gain insight into the structure-function relationship of the SLC6 family members. There is a consensus that

LeuT has two Na^+ sites that are part of an allosteric network that regulates Na^+-coupled amino acid symport [6,10,11]. However, to obtain a better understanding of how ions, such as Na^+, that are at the resolution of crystallographic approaches, coordinate protein function, it is critical to developing methods to facilitate their unequivocal identification in protein structures.

Assignment of ions into the electron density of X-ray crystallography or the coulomb map of cryo-EM is not trivial. They can be confused with water molecules or other solvent components, and this is especially true for ions such as Na^+ and Mg^{2+} with low atomic numbers (e.g., when $Z \leq 20$) and when they are only partially occupied in a protein. Anomalous scattering is a powerful method to identify low-Z anomalous scattering elements in a crystal structure [12–14], but it is often difficult to identify low-Z elements where it may not be readily feasible to perform anomalous scattering experiments across the relevant absorption edge. To this end, we developed an f″ refinement method for the identification of low-Z elements in our native-SAD structures [14]. We have also used the f″ refinements to identify ions in studies of ion channels, notably so for vertebrate TRIC channels [15] and a putative bacterial ion channel TehA [16]. However, the identification of Na^+ is particularly challenging since its anomalous scattering is very weak at the available wavelength at synchrotron sources (f″ = 0.22e at 6 keV). To address this issue, we recently devised a multi-crystal assembly and rejection strategy using low-energy X-rays to enhance anomalous signals from off-resonance weak scatterers [17–19]. Here, we describe the optimization of the low-energy multi-crystal approach using 5 keV X-rays for studying anomalous diffraction from native LeuT crystals. Using this approach, we experimentally identified two Na^+ in the two Na^+ sites (termed Na1 and Na2) in LeuT. We also performed Na^+ depletion experiments to explore Na^+-mediated conformational changes in the LeuT transport cycle. This approach can be applied for the identification of ions, e.g., Na^+, in low-resolution crystal structures as well as to monitor protein conformational changes upon Na^+ depletion by using time-resolved serial crystallography.

2. Materials and Methods

2.1. Protein Purification, Characterization, and Crystallization

LeuT from *Aquifex aeolicus* (UniProt accession number O67854) was cloned into a pNYCOMPS-C23 vector [20] including a C-terminal TEV cleavage site followed by a 10xHis-tag. LeuT was expressed in *E. coli* C41 (DE3) (ThermoFisher Scientific, Waltham, MA, USA), cultured in terrific broth, after inducing gene expression by the addition of 0.3 mM isopropyl-β-D-thiogalactopyranoside (IPTG) at an absorbance of 0.5 at 600 nm (A600) at 20 °C for 20 h. Cells were disrupted by using an Emulsiflex C3 (Avestin) and membranes were collected by ultracentrifugation at 185,000× *g*, 4 °C for 1 h. Membrane pellets were washed twice with 200 mM Tris/MES, pH 7.5, 0.1 mM TCEP, and 5% glycerol and solubilized with 30 mM n-dodecyl-β-D-maltopyranoside (DDM) for 2 h at 4 °C. Insoluble material was removed by ultracentrifugation at 4 °C, 185,000× *g* for 40 min. LeuT was purified by IMAC employing Ni-chelating resin (G-biosciences, St Louis, MO, USA) and eluted in 50 mM Tris/MES, pH 7.5, 5% glycerol, 150 mM NaCl, 400 mM Imidazole, 0.1 mM TCEP, and 0.5 mM DDM. The C-terminal His-tag was removed by overnight TEV digestion at 4 °C followed by size exclusion chromatography using a Superdex increase 200 10/300 GL column (GE Healthcare) equilibrated in 10 mM Tris, pH 8.0, 45 mM NaCl, 5 mM KCl, and 40 mM n-octyl-β-D-glucopyranoside (OG). Peak fractions containing LeuT were pooled. For crystallization, the pooled fraction was concentrated to 7 mg/mL with a Vivaspin 50 kDa cutoff centrifugal concentrator (SARTORIUS, Göttingen, Germany). Concentrated LeuT was mixed with 0.1 M HEPES pH 7.0, 100 mM NaCl, 20–25% PEG 550 MME in a ratio of 1:1 (*v*/*v*) for crystallization by a sitting-drop method at 19 °C. Microcrystals of LeuT grew in a few days and were harvested by centrifugation at 500× *g* for 5 min followed by the removal of the supernatant. Microcrystals were then resuspended in a stabilization buffer consisting of 0.1 M HEPES, pH 7.0, 100 mM NaCl, 20–25% PEG 550 MME, and 0.5 mM DDM. Microcrystals of LeuT were dehydrated by increasing the PEG 550 MME

concentration to 30% with 2.5% increment steps. We used low-background polyimide loops with only one crystal in each loop. To reduce the low-energy X-ray absorption of the buffer, we removed the buffer from around the crystals using filter paper. Dehydrated LeuT microcrystals were cryo-cooled in liquid nitrogen for diffraction data collection.

For functional characterization, LeuT was purified as described above without the removal of the His-tag. To assess the effect of 'trapped' Na^+ and Leu in LeuT preparations that are known to remain bound from the cell culture and prevent binding of Na^+ and Leu to their respective binding sites [6,21], membrane vesicles of *E. coli* C41 (DE3) expressing LeuT were subjected to the treatment with 10 mM Crown-5 (Sigma-Aldrich, St. Louis, MI, USA) prior to the purification of LeuT. The activity of purified LeuT was assessed using scintillation proximity assay (SPA)-based binding of 50 nM ^{3}H-Leu (120 Ci/mmol) (American Radiolabeled Chemicals, Inc. St. Louis, MI, USA) in assay buffer composed of 100 mM Tris/MES pH 7.5, 50 mM NaCl (or 150 mM Tris/MES for Na^+-free conditions), 0.1 mM TCEP, 5% glycerol, and 5 mM DDM using 1.25 mg/mL of copper-coated YSi-SPA beads (Perkin Elmer, Waltham, MA, USA) to immobilize His-tagged LeuT. The background binding activity, i.e., the non-proximity signal (NPS), was assessed by performing the assay in the presence of 800 mM imidazole which competes with the His-tag for binding to the SPA beads. Samples were measured in a photomultiplier-tube-based microwell counter as described [22] and shown as counts per minute (cpm).

2.2. Crown-5 Soaking

To remove Na^+ from LeuT crystals, soaking experiments were performed at 4 °C. Crown-5 at a stock concentration of 100 mM was diluted to 1 mM, 3 mM, 5 mM, and 10 mM in a soaking buffer containing 0.1 M HEPES pH 7.0, 20–25% PEG 550 MME, and 0.5 mM DDM. For soaking in different Crown-5 concentrations, microcrystals were repeatedly (three times) incubated with the soaking solution for 5 min followed by centrifugation to remove the soaking buffer. The soaked crystals were used for dehydration to a final 30% PEG 550 MME with a step of 2.5%. We mounted crystals using the same strategy as native LeuT crystals. Soaked and dehydrated LeuT microcrystals were cryo-cooled in liquid nitrogen for diffraction data collection.

2.3. Diffraction Data Collection

Both native LeuT and Crown-5-soaked data sets were collected at the FMX beamline at National Synchrotron Light Source II (NSLS-II) with a cryostream operated at 100 K [23]. The FMX beamline is equipped with a DECTRIS Eiger X 16M detector (DECTRIS USA, Inc., Philadelphia, PA, USA). To reduce the background and absorption of X-rays at low energy, polyimide loops were used and buffer around the crystals was removed by paper [17]. Raster scans were used for identifying well-diffracting microcrystals. To limit X-ray absorption at low energy, we used only crystals of about 30 microns in size. Crystals were of rod shape which allowed us to collect 600 frames using a vector data collection method with 0.3 degrees per 0.02 sec exposure time. The X-ray energy was moved to 5 keV (wavelength = 2.48 Å) for enhanced anomalous signals from Na^+. The beam size is 5 × 6 µm (V × H). For each Crown-5-soaked LeuT crystal, diffraction data were collected at a sample-to-detector distance of 140 mm, and an exposure time of 0.02 sec per frame for a total of 600 frames.

2.4. Data Reduction and Assembly

Seventy single crystal data sets (600 frames for each crystal) were indexed and integrated independently as 10 accumulated wedges per crystal (1–60, 1–120, . . . , 1–600) using PyMDA [19] which integrates the software DIALS, POINTLESS, and AIMLESS [24–27]. All wedges were scaled, and the largest wedges which have a CC1/2 value above 0.9 at 4 Å were chosen for each crystal. Seventy single-crystal data sets were classified based on the variation of their unit cell parameters [28]. Among them, 35 crystals in cluster 4 (UC4) had acceptable diffraction quality and were used for downstream assembly in PyMDA

(Figure 1a). To remove outlier crystals, crystal rejection was performed one by one from the 35 crystals using PyMDA, resulting in 32 crystals for the final data assembly. The assembled data sets after each crystal rejection were further subjected to a different extent of frame rejection by using PyMDA (Figure 1b). The extent of frame rejection is defined by frame_cutoff = [min(SmRmerge) × (1 + decay)], where min(SmRmerge) is the lowest SmRmerge, reported by AIMLESS, within a single-crystal data set; and decay is a rejection ratio of none, 500%, 400%, 300%, 200%, and 100%. Frames with SmRmerge larger than frame_cutoff were excluded from the assembly in AIMLESS. For example, 200% indicates that frames with a SmRmerge of 200% more than min(SmRmerge) are rejected from scaling and merging [18,19]. Data reduction and assembly statistics are shown in Table 1.

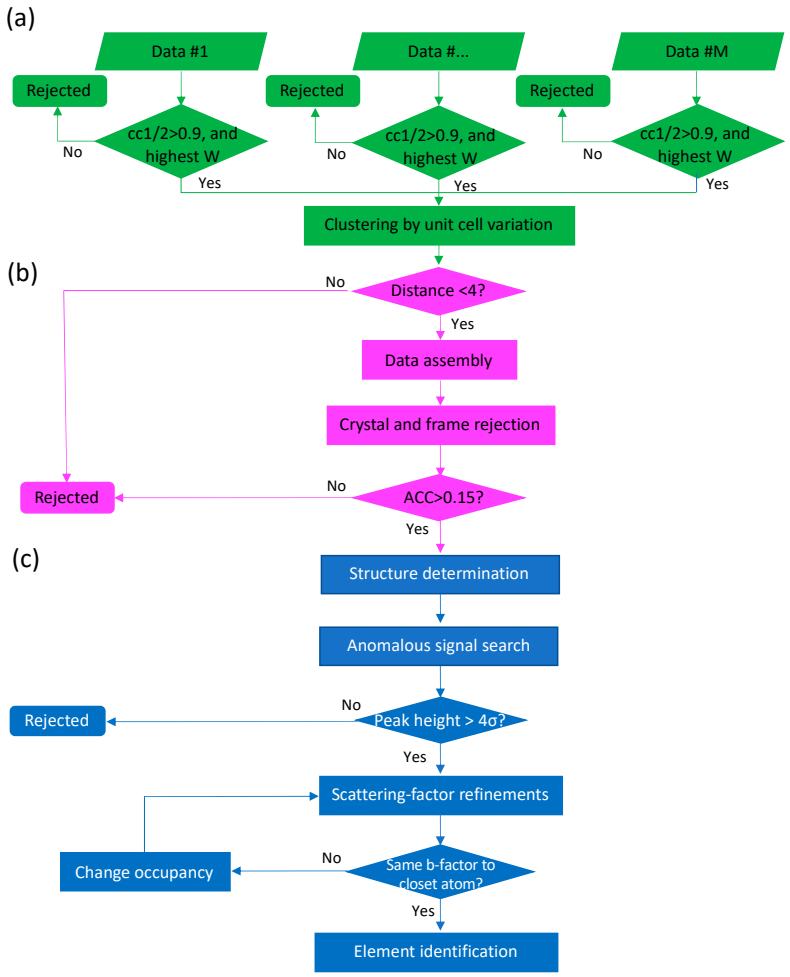


Figure 1. Schematic workflow for Na^+ identification. (**a**) Single-crystal data set processing. Single-crystal data sets were independently indexed, integrated, and scaled using PyMDA as 10 progressively accumulated wedges (W) (W1, 1–60; W2, 1–120; . . . , W10, 1–600 frames). The largest wedges which have CC1/2 > 0.9 were selected for further data analysis. (**b**) Data assembly and rejection. Data sets classified with a unit-cell variation of less than 4 were combined. Unit-cell variation is defined as Euclidean distances normalized by population variances as reported previously [28]. Assembled data sets were subjected to crystal rejection followed by frame rejection by PyMDA. Only data sets that showed significant anomalous signals (ACC > 0.15) were advanced to the next step. (**c**) LeuT structure was determinized by molecular replacement using PDB code 3GJD as a search model. Anomalous signals were searched by ANODE. Significant anomalous signals (>4σ) at the Na^+ binding site were subjected to f″ refinement by PHENIX.REFINE. The occupancy of anomalous scatterers was changed from 1.0 to 0.1 in 0.1 intervals to get refined individual B-factor and f″ values. The refined f″ value of an anomalous scatterer that has a B-factor value closest to its neighboring atom(s) was selected. The element was assigned by comparing the refined f″ value with its theoretical value at 5 keV.

Table 1. Data collection and refinement statistics.

Data Collection	LeuT (Multi-Crystals)	LeuT w Crown-5
Beamline	FMX (NSLS-II)	FMX (NSLS-II)
Wavelength (Å)	2.48	2.48
Space group	C2	C2
Unit cell (Å)		
a, b, c (Å)	87.11, 86.38, 80.73	86.44, 87.38, 80.80
a, b, γ (°)	90.0, 95.3, 90.0	90.00, 95.1, 90.00
Solvent content (%)	53.2	53.5
Bragg spacings (Å)	38.04–4.001 (4.144–4.001)	39.44–3.8 (3.936–3.8)
Total reflections	595,518 (60,371)	19,702 (1975)
Bijvoet unique reflections	10,240 (1028)	11,251 (594)
Completeness (%)	99.65 (100.00)	98.50 (98.99)
<I/σ(I)>	26.6 (21.3)	2.3 (0.7)
R_{split}	0.027	0.272
Multiplicity	116 (117.9)	3.3 (3.3)
$CC_{1/2}$	0.997 (0.996)	0.982 (0.535)
Refinement		
Resolution (Å)	4	3.8
No. reflections	5110 (514)	5911 (589)
R_{work}/R_{free}	0.169/0.201	0.272/0.315
No. atoms	4263	4056
Wilson *B* factor ($Å^2$)	60.79	122.14
Average *B* factor ($Å^2$)	55.7	125.05
R.m.s. deviations		
Bond length (Å)	0.004	0.002
Bond angle (°)	0.69	0.49
PDB code	8FT4	8FT5

2.5. Structure Determination and Low-Z Element Identification

Data sets that showed significant anomalous signals (anomalous correlation coefficient (ACC) > 0.15) were used for structure determination by molecular replacement employing PHENIX.PHASER [29] using PDB code 3GJD as a searching model [30]. Iterative model building and refinement were performed by using the program COOT [31] and PHENIX.REFINE [32], respectively. Bijvoet-difference Fourier maps and peak heights were calculated using ANODE [33]. f″ values for anomalous scatterers were obtained through the f″ refinement (Figure 1c) [14] using PHENIX.REFINE [32]. For the f″ refinement, we changed the occupancy of anomalous scatterers from 1.0 to 0.1 in 0.1 intervals and refined individual B-factor and f″ values. The refined f″ value of an anomalous scatterer that has a B-factor value closest to its neighboring atom(s) was selected. The stereochemistry of the refined structures was validated by using the programs MolProbity [34] and PHENIX.REFINE. Structural refinement and validation statistics are listed in Table 1.

3. Results

3.1. Anomalous Diffraction of Na^+ in LeuT

LeuT is a model transporter employed to understand the molecular mechanism of the SLC6 family of the NSS. LeuT, a representative for NSS, utilizes the electrochemical gradient to mediate Na^+-coupled solute symport [10]. The original LeuT structure (PDB code: 2A65) [6] revealed the presence of two Na^+, and functional studies revealed the importance of the two Na^+ in the Na1 and Na2 sites for regulating LeuT conformational transitions that appear to be the core of the transport cycle [5,10]. The crystallographic characterization of the two Na^+ by anomalous diffraction in LeuT provids a stepping stone to gaining insight into the transport mechanism in LeuT and the SLC6 family transporters. However, the K absorption edge of Na^+ is 1.07 keV (http://skuld.bmsc.washington.edu/scatter/AS_periodic.html (accessed on 17 January 2023)), which is not accessible at any synchrotron crystallography facility. The lowest energy reported so far is 2.5 keV near

the sulfur edge at the Diamond Light Source I23 [35]. We have recently developed a multi-crystal assembly strategy to enhance anomalous signals from off-resonance weak scatterers [16,19], and we, therefore, explored this method for the characterization of Na^+ anomalous diffraction in LeuT (Figure 1).

We initially used 6 keV X-rays, which are commonly used for native-SAD phasing of protein crystals of decent size [36]. However, we could not detect any anomalous signals from the Na^+ binding site in LeuT. To exploit the increased anomalous diffraction of Na^+ at lower energy, we choose to use 5 keV to enhance Na^+ anomalous signals (f″ = 0.31e at 5 keV vs. 0.22e at 6 keV) and microcrystals to reduce the absorption of low-energy X-rays [37]. We collected 70 single-crystal data sets but none of the individual data sets showed significant anomalous signals. To enhance weak anomalous signals, we performed unit-cell variation analysis to find out compatible clusters for data assembly [28] (Figure 2a). Those data sets were classified into four clusters (named UC1-4), UC1-3 have divergent unit-cell parameters compared to our reference LeuT structure (PDB code: 3GJD), and the largest cluster (UC4) has the closest unit-cell parameters (Figure 2a). The UC4 cluster showed the best data quality with a resolution beyond 4.0 Å. We hence used UC4 data sets for assembly. Figure 2b,c shows the data quality of the assembled data sets under different rejection conditions. Most of the data sets show high CC1/2 (>98%) and low Rsplit (<10%) values, confirming that these crystals were compatible with assembly. The anomalous signals (reported as anomalous correlation coefficient, ACC) significantly increased with the increased number of assembled crystals (Figure 2d).

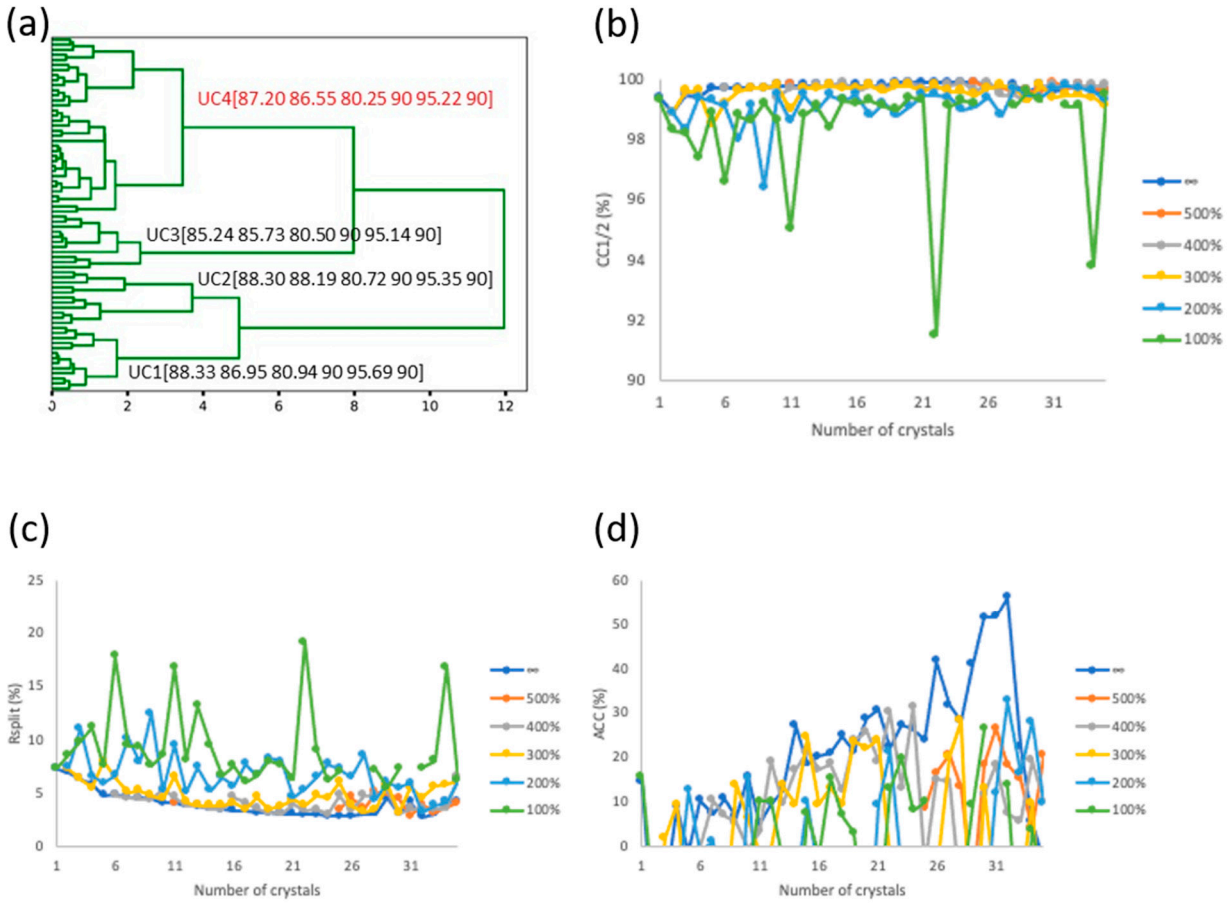


Figure 2. Data analysis of assembled LeuT data sets. (**a**) Unit-cell variation analysis for classification of single-crystal data sets. Unit-cell parameters of each cluster are shown. (**b**–**d**) Data assembly and subsequent crystal and frame rejections were performed by using PyMDA as described in the methods: ∞, no frame rejection and 500–100%, where 100% is the most stringent rejection. (**b**) CC1/2 at 4 Å d_{min}. (**c**) Rsplit at 4 Å d_{min}. (**d**) Anomalous correlation coefficient (ACC) at 10 Å d_{min}.

3.2. Speciation of Anomalous Scattering Elements in LeuT

The LeuT structure was solved by molecular replacement from assembled data set which showed significant anomalous signals (ACC > 0.15), and anomalous scatterers were searched in the solved structure by ANODE. Figure 3a shows anomalous difference in Fourier peak heights from the 32-crystal data set which showed the highest anomalous signals (Figure 2d). We were able to identify 19 peaks above 4.0σ including 11 sulfur (peaks 1–10 and 12), 1 chloride ion (peak 14), and 1 unknown (peak 11) (Figure 3b). Importantly, peaks 13 and 16 have positions identical to the two Na^+ ions in the LeuT structure [30]. The distances between the Na^+ peaks and coordinating atoms are 2.3–2.5 Å, which is appropriate for Na^+ coordination (Figure 3d). Therefore, we conclude that these two peaks correlate to the two Na^+ in LeuT.

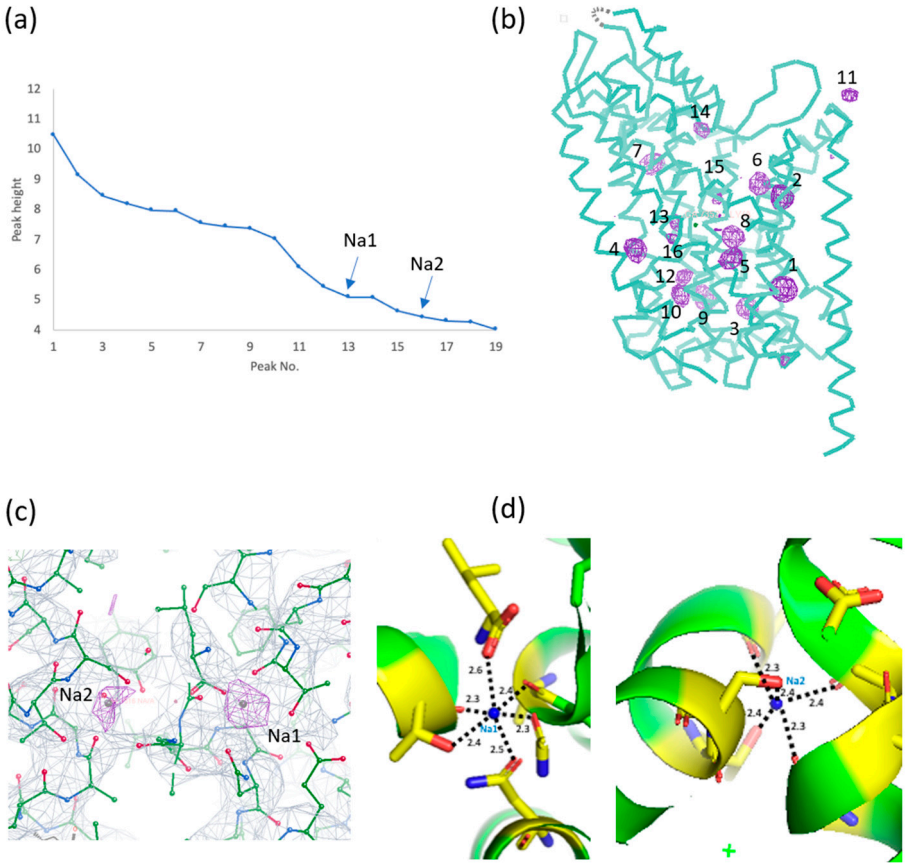


Figure 3. Characterization of Na^+ in LeuT. (**a**) A plot of the 19 highest Bijvoet-difference Fourier peaks in LeuT. Two Na^+ peaks are indicated by arrows. (**b**) Bijvoet-difference Fourier peaks are shown as purple isomeshes contoured at 3.5σ. The refined LeuT model is shown as sticks. Sulfur peaks for methionine residues are 1, M363; 2, M403; 3, M65; 4, M199; 5, M360; 6, M394; 7, M44; 8, M176; 9, M452; 10, M18; 12, M59. Peaks 13 and 16 are for Na1 and Na2, respectively. Peaks 11 and 14 were identified as Cl^- (**c**) Electron densities (magenta isomeshes contoured at 4σ) for two Na^+ in LeuT. 2Fo-Fc electron densities are shown as grey isomeshes contoured at 1.5σ. (**d**) Na^+-binding sites in LeuT. Residues and leucine forming the Na^+-binding sites are shown as sticks. Distances (Å) between Na^+ and the bound atoms are shown as dash lines.

To specify the element for each identified anomalous difference Fourier peak, we performed f″ refinement using PHENIX.REFINE [32]. Since the f″ value depends on occupancy, we varied occupancy of each anomalous scatterer for refinement and the approximate f″ value was determined where B-factor values of surrounding atoms are closest to the scatterer (Table 2). We found approximate f″ values were 0.32e for Na1 (occupancy 0.9) and 0.36e for Na2 (occupancy 0.8), that are almost identical to the theoretical

f″ value of 0.31e for Na^+ at 5 keV. We also found approximate f″ values of 1.45e for Cl^-, (peak 14, which was previously identified as Cl^- that was proposed to have no functional relevance for the transport process [6]) and 1.36e for the unknown peak 11. Because the theoretical f″ value is 1.63e for Cl^- at 5 keV, peak 11 is likely another Cl^- which was not previously reported. The other possibility for peak 11 is P or K which existed in our crystallization mother liquor. However, the theoretical f″ values are 1.04e for P and 2.4e for K at 5 keV, which are away from 1.45e (peak 14) and 1.36e (peak 11). Furthermore, peak 11 is coordinated by the N atoms from His480 and Trp481. Therefore, the unknown peak 11 may be assigned as Cl^-. Taken together, our crystallographic analysis of anomalous scatterers in LeuT directly resolved the presence of two Na^+ in the immediate proximity of the central leucine binding site of LeuT as previously proposed [6]. In addition, we identified a new Cl^- from the unknown peak 11, which, due to its remote location relative to the core network of the substrate and Na^+ binding sites, appears to have no physiological role for LeuT-mediated substrate transport.

Table 2. Scattering-factor refinements for anomalously scattering elements. f″(S) shows the average value of all sulfur scatterers. Refined f″ values are in bold.

Occupancy	f″(Na1)	f″(Na2)	f″(Cl)	f″(Peak11)	f″(S)
1	0.16	0.20	1.33	0.51	**1.05**
0.9	**0.32**	0.33	1.21	0.52	1.13
0.8	0.37	**0.36**	1.25	0.62	1.21
0.7	0.43	0.39	1.32	0.69	1.27
0.6	0.50	0.45	**1.45**	0.80	1.42
0.5	0.57	0.55	1.61	0.91	1.58
0.4	0.71	0.54	1.84	1.09	1.94
0.3	0.89	0.56	2.15	**1.36**	2.30
0.2	0.88	0.61	2.24	1.48	2.69
0.1	0.41	0.38	1.22	0.79	2.97

3.3. Characterization of Na^+ in LeuT

We found Na1 has stronger anomalous signals compared to Na2 (Figure 3c). The occupancy of Na1 (0.9) is also higher than Na2 (0.8) (Table 2). This result is consistent with the computational study of Na1 and Na2 occupancy in the presence of substrate leucine [38]. Na1 has an octahedral coordination while Na2 has only a four-atom coordination (Figure 3d). Therefore, compared to Na2, Na1 may have a higher affinity as suggested by a higher occupancy and peak height. However, the Na2 site is highly conserved in the majority of proteins sharing the conserved LeuT fold architecture [39]. In H^+-coupled symporters that feature the LeuT fold, a positively charged residue occupies the space that aligns with the Na2 site in the Na^+-dependent systems, indicating that a positive charge, originating from the Na^+ in the Na2 site or from a positively charged amino acid side chain may be involved in ion coupling [40–43]. In comparison, the Na1 site in LeuT-fold transporters is less conserved which may reflect the flexibility of the Na1 binding site to accommodate diverse substrates in the adjacent substrate binding site [44].

3.4. Conformational Change upon Na^+ and Substrate Depletion

Na^+-free LeuT is unstable at a physiological pH. Therefore, stabilization strategies such as mutations, low pH, and the use of Fab fragments were employed to obtain LeuT structures in apo conformations [45,46]. Here, we took a different approach to obtain LeuT structures in an apo conformation (i.e., Na^+-free) at a more physiological pH (pH of 7.0) by removing Na^+ in LeuT crystals using Crown-5, a Na^+-chelating compound [47]. We initially tried to soak large crystals with Crown-5, but those crystals were cracked and could not be used for diffraction data collection, suggesting that Na^+ depletion from LeuT crystals caused conformational changes and destroyed the crystal lattice. To overcome this issue, we used microcrystals of 10–20 μm in size. We hypothesized that microcrystals

may tolerate the conformational changes induced by the diffusion of Crown-5 and Na^+. As we expected, microcrystals survived after soaking with Crown-5 at a concentration of 3 mM. These soaked microcrystals preserved diffraction quality at 3.8 Å resolution (Table 1). Compared to the Na^+ and Leu-bound LeuT structure, the structure we obtained after Crown-5 soaking shows a significant loss of electron densities for the substrate Leu (Figure 4a). This observation is consistent with the fact that Leu can only bind to LeuT in the presence of Na^+ [10]. Removing Na^+ from the assay medium impaired ^{3}H-Leu binding to LeuT (Figure 4b). Because the anomalous signals from a single crystal are weak and the resolution is low, we cannot use anomalous difference Fourier peaks or Fo-Fc electron densities to validate the depletion of Na1 and Na2. Our result nevertheless indicates that most of Na1 were removed by Crown-5 so Leu binding was weakened. The depletion of Leu did not yield observable conformational changes of the Na1 and Na2 sites, consistent with the previously determined apo LeuT structure [45] and functional data that show that binding of $^{22}Na^+$ to LeuT is indistinguishable in the presence or absence of Leu [10].

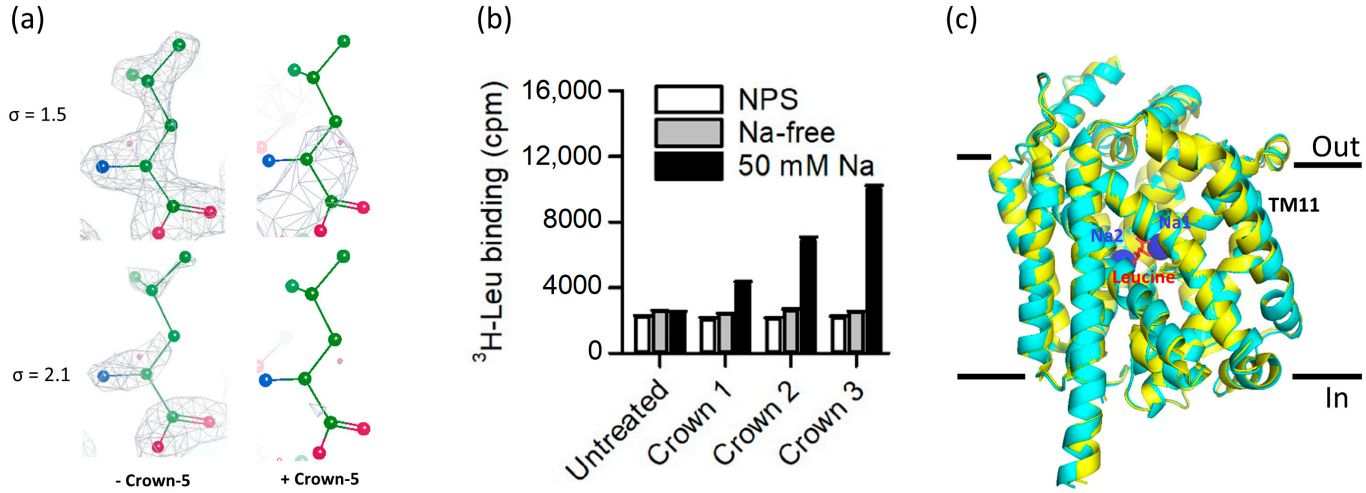


Figure 4. Na^+ and leucine depletion in LeuT. (**a**) 2Fo-Fc electron density maps of bound substrate leucine with and without Crown-5 soaking. (**b**) Removal of Na^+ from LeuT-containing *E. coli* C41(DE3) membrane vesicles by repeated treatments with Crown-5 as described in the Methods. The activity of 50 ng of purified LeuT from differently treated vesicles was then assessed by measuring the binding of 50 nM ^{3}H-Leu (120 Ci/mmol) in the presence of 50 mM NaCl (50 mM Na; black bars) or the absence of NaCl (Na-free; gray bars) in the assay buffer using the scintillation proximity assay (SPA). The non-proximity signal (NPS) was determined for each condition. Na^+ and Leu from the cell culture medium are trapped in LeuT and prevent significant binding of ^{3}H-Leu to the untreated sample. Repeated treatments with Crown-5 during the vesicle preparation led to the removal of the trapped compounds. Data are the mean ± S.E.M of three independent repeats that were performed as technical triplicates. (**c**) Comparison of LeuT structure with (yellow) and without (cyan) Crown-5 soaking (PDB code: 3GJD). Two Na^+ and the substrate leucine in the non-soaking structure (PDB code 3GJD) are shown as blue spheres and red sticks, respectively.

Figure 4c shows the conformational difference between LeuT structures with and without Crown-5 soaking. Compared with the Na^+- and Leu-bound LeuT structure (PDB code: 3GJD), the Crown-5-soaked structure has an R.M.S.D. of 0.405 Å for aligned Cα atoms. Remarkably, substantial relocation was observed in TM11, indicating that it is involved in a conformational change upon Na^+ or Leu depletion. The structure we determined is in a substrate/Na^+-bound occluded conformation. The depletion of Na^+ and Leu and the conformational change in TM11 might trigger an inward-facing conformation, favoring Na^+ and Leu release in the LeuT transport cycle. Our Crown-5 soaking experiment demonstrates that microcrystals offer applications for exploring membrane protein conformational changes upon soaking without destroying crystal lattice and diffraction quality.

4. Discussion

Identification of biologically relevant low-Z ions (Na^+, Mg^{2+}, K^+, Ca^{2+}, Cl^-, PO_4^{2-}, SO_4^{2-}) in a crystal structure gives important clues to understanding their interactions with proteins and provides critical leads to their functional or regulatory roles in protein physiology. However, the K edge of these low-Z ions is not accessible at most of the synchrotron facilities. Therefore, it is difficult to directly identify these low-Z ions by anomalous scattering because of their low f″ value at an off-resonance wavelength. As a compromise, heavier ions with much higher f″ values and similar chemical characters were commonly used as surrogates such as Rb^+ or Tl^+ for K^+, Os^{3+} for Mg^{2+}, WO_4^{2-} for PO_4^{2-}, SeO_4^{2-} for SO_4^{2-}, Br^- or I^- for Cl^-, and Yb^{3+} for Ca^{2+} [48–51]. However, the use of non-native ions may lead to different coordination and misinterpretation. A notable example occurs in the classic KcsA channel, where K^+ sites in the selectivity filter appeared to be half occupied in mechanistically relevant pairs using TI^+ instead of K^+ [50]. Wagner's group has revisited this problem using K^+ anomalous scattering to determine its occupancy and showed that the selectivity filter is fully occupied by K^+ [52]. For Na^+, there are no surrogates. Na^+ has 10 electrons which are close to oxygen's eight electrons in water. Therefore, the identification of Na^+ from water in a crystal structure remains a challenge. Recently, we published the native-SAD structure of TehA using a multi-crystal assembly method at 5 keV, and we identified an unknown anomalous peak as Na^+ [16]. In this work, we applied this method to allow for the first time, visualization of anomalous scattering from the two Na^+ in LeuT. We demonstrated that using X-rays at 5 keV, Na^+ can be resolved from its anomalous diffraction signals (Figure 3).

The theoretical f″ for Na^+ is 0.31e at 5 keV. The anomalous signals of Na^+ in our 5-keV diffraction data were very weak. Typically, we observed many noisy anomalous signals below a peak height at 4σ. The noise may be decreased by averaging data from multiple crystals. To identify Na^+ in LeuT, we averaged data from 32 crystals to boost Na^+ anomalous signals with peak heights of above 4σ. We also found the Na^+ peak height depends on resolution cut-offs because the noise is higher in higher-resolution data. To find a suitable resolution cutoff, we processed data at 2.8 Å, 3.5 Å, and 4.0 Å. The highest Na^+ peak height came from the 4.0 Å cut-off data.

Once the anomalous peaks for Na^+ were identified, f″ refinement using PHENIX.REFINE can refine both B-factor and Na^+ f″ values simultaneously, which allowed us to assign and verify both Na^+ in LeuT. Therefore, our Na^+-identification method for LeuT paves the way for the identification of Na^+ and other weakest anomalous scatterers using 5 keV X-rays and a multi-crystal assembly strategy as illustrated in Figure 1.

LeuT operates the transport of amino acids via an alternating access model, which includes three major conformations, outward-open, occluded, and inward-open state [5]. Although capturing high-resolution snapshots of intermediates along the transport cycle is a daunting task, these major states have been revealed by crystal structures [6,11,45,46]. Among them, however, apo states are unstable and stabilization with mutation, Fab binding or non-physiological conditions (low pH) was necessary to solve the structures [45,46]. Here we used Crown-5 to remove Na^+ in LeuT microcrystals at a physiological pH of 7.0 to capture an apo state absent of both Na^+ and substrate. Although we could not verify the complete depletion of Na^+ in our crystallographic approach, we found that the electron density coverage for the substrate leucine was reduced by Crown-5 soaking. This result, together with functional studies (Figure 4b), indicates that Na^+ is required to enable leucine binding.

5. Conclusions

Crystallographic characterization of Na^+ in the NSS member LeuT remains a challenge due to its extremely weak anomalous diffraction signals. We used 5-keV X-rays in conjunction with multiple crystals and optimized data analysis to boost Na^+ anomalous diffraction peak heights from the otherwise background noise. At above 4σ, we identified and verified two Na^+ in LeuT through f″ refinement. We also demonstrate that Na^+ depletion by its chelator Crown-5 from microcrystals led to an apo structure free of Na^+ and

substrate. The element identification method presented in this work can be used to discover Na^+ which is abundant in many membrane and soluble proteins, reflective of its central biological function.

Author Contributions: Conceptualization, A.K. and Q.L.; formal analysis, A.K., M.Q., W.A.H. and Q.L.; investigation, A.K., H.L., M.Q. and Q.L.; writing of original draft preparation, A.K. and Q.L.; writing of review and editing, A.K., M.Q., W.A.H. and Q.L.; visualization, A.K.; supervision, Q.L.; project administration, W.A.H. and Q.L. All authors have read and agreed to the published version of the manuscript.

Funding: This research was funded in part by NIH grants GM107462 and P41GM116799.

Institutional Review Board Statement: The study did not require ethical approval.

Informed Consent Statement: Not applicable.

Data Availability Statement: Atomic coordinates and structure factor files have been deposited in the RCSB Protein Data Bank (PDB) under the accession codes 8FT4 for native LeuT and 8FT5 for LeuT soaked with Crown-5.

Acknowledgments: We thank the staff at the NSLS-II FMX beamline for their assistance in data collection. The FMX beamline is part of the Center for BioMolecular Structure (CBMS) which is primarily supported by the National Institutes of Health, National Institute of General Medical Sciences (NIGMS) through a Center Core P30 Grant (P30GM133893), and by the DOE Office of Biological and Environmental Research (KP1607011). NSLS-II is supported in part by the U.S. Department of Energy, Office of Science, Office of Basic Energy Sciences Program under contract number DESC0012704 (KC0401040).

Conflicts of Interest: The authors declare no conflict of interest.

References

1. Bie, P. Mechanisms of sodium balance: Total body sodium, surrogate variables, and renal sodium excretion. *Am. J. Physiol. Integr. Comp. Physiol.* **2018**, *315*, R945–R962. [CrossRef] [PubMed]
2. Gagnon, K.B.; Delpire, E. Sodium Transporters in Human Health and Disease. *Front Physiol* **2020**, *11*, 588664. [CrossRef] [PubMed]
3. Serrano, R. Salt tolerance in plants and microorganisms: Toxicity targets and defense responses. *Int. Rev. Cytol.* **1996**, *165*, 1–52. [PubMed]
4. Vasak, M.; Schnabl, J. Sodium and Potassium Ions in Proteins and Enzyme Catalysis. *Met. Ions. Life Sci.* **2016**, *16*, 259–290. [PubMed]
5. Del Alamo, D.; Meiler, J.; McHaourab, H.S. Principles of Alternating Access in LeuT-fold Transporters: Commonalities and Divergences. *J. Mol. Biol.* **2022**, *434*, 167746. [CrossRef] [PubMed]
6. Yamashita, A.; Singh, S.K.; Kawate, T.; Jin, Y.; Gouaux, E. Crystal structure of a bacterial homologue of Na+/Cl–dependent neurotransmitter transporters. *Nature* **2005**, *437*, 215–223. [CrossRef]
7. Zeppelin, T.; Ladefoged, L.K.; Sinning, S.; Schiott, B. Substrate and inhibitor binding to the serotonin transporter: Insights from computational, crystallographic, and functional studies. *Neuropharmacology* **2019**, *161*, 107548. [CrossRef]
8. Colas, C. Toward a Systematic Structural and Functional Annotation of Solute Carriers Transporters-Example of the SLC6 and SLC7 Families. *Front Pharmacol.* **2020**, *11*, 1229. [CrossRef]
9. Freissmuth, M.; Stockner, T.; Sucic, S. SLC6 Transporter Folding Diseases and Pharmacochaperoning. *Handb Exp. Pharm.* **2018**, *245*, 249–270.
10. Shi, L.; Quick, M.; Zhao, Y.; Weinstein, H.; Javitch, J.A. The mechanism of a neurotransmitter:sodium symporter–inward release of Na+ and substrate is triggered by substrate in a second binding site. *Mol. Cell* **2008**, *30*, 667–677. [CrossRef]
11. Gotfryd, K.; Boesen, T.; Mortensen, J.S.; Khelashvili, G.; Quick, M.; Terry, D.S.; Missel, J.W.; LeVine, M.V.; Gourdon, P.; Blanchard, S.C.; et al. X-ray structure of LeuT in an inward-facing occluded conformation reveals mechanism of substrate release. *Nat. Commun.* **2020**, *11*, 1005. [CrossRef] [PubMed]
12. Einsle, O.; Andrade, S.L.; Dobbek, H.; Meyer, J.; Rees, D.C. Assignment of individual metal redox states in a metalloprotein by crystallographic refinement at multiple X-ray wavelengths. *J. Am. Chem. Soc.* **2007**, *129*, 2210–2211. [CrossRef] [PubMed]
13. Spatzal, T.; Schlesier, J.; Burger, E.M.; Sippel, D.; Zhang, L.; Andrade, S.L.; Rees, D.C.; Einsle, O. Nitrogenase FeMoco investigated by spatially resolved anomalous dispersion refinement. *Nat. Commun.* **2016**, *7*, 10902. [CrossRef] [PubMed]
14. Liu, Q.; Liu, Q.; Hendrickson, W.A. Robust structural analysis of native biological macromolecules from multi-crystal anomalous diffraction data. *Acta Cryst. D Biol Cryst.* **2013**, *69 Pt 7*, 1314–1332. [CrossRef] [PubMed]
15. Wang, X.H.; Su, M.; Gao, F.; Xie, W.; Zeng, Y.; Li, D.L.; Liu, X.L.; Zhao, H.; Qin, L.; Li, F.; et al. Structural basis for activity of TRIC counter-ion channels in calcium release. *Proc. Natl. Acad. Sci. USA* **2019**, *116*, 4238–4243. [CrossRef] [PubMed]

16. Karasawa, A.; Andi, B.; Fuchs, M.R.; Shi, W.; McSweeney, S.; Hendrickson, W.A.; Liu, Q. Multi-crystal native-SAD phasing at 5 keV with a helium environment. *IUCrJ* **2022**, *9 Pt 6*, 768–777. [CrossRef]
17. Guo, G.; Fuchs, M.R.; Shi, W.; Skinner, J.; Berman, E.; Ogata, C.M.; Hendrickson, W.A.; McSweeney, S.; Liu, Q. Sample manipulation and data assembly for robust microcrystal synchrotron crystallography. *IUCrJ* **2018**, *5 Pt 3*, 238–246. [CrossRef]
18. Guo, G.; Zhu, P.; Fuchs, M.R.; Shi, W.; Andi, B.; Gao, Y.; Hendrickson, W.A.; McSweeney, S.; Liu, Q. Synchrotron microcrystal native-SAD phasing at a low energy. *IUCrJ* **2019**, *6 Pt 4*, 532–542. [CrossRef]
19. Takemaru, L.; Guo, G.; Zhu, P.; Hendrickson, W.A.; McSweeney, S.; Liu, Q. PyMDA: Microcrystal data assembly using Python. *J. Appl. Crystallogr.* **2020**, *53 Pt 1*, 277–281. [CrossRef]
20. Bruni, R.; Kloss, B. High-throughput cloning and expression of integral membrane proteins in *Escherichia coli*. *Curr. Protoc. Protein. Sci.* **2013**, *74*, 29.6.1–29.6.34. 2. [CrossRef]
21. Quick, M.; Shi, L.; Zehnpfennig, B.; Weinstein, H.; Javitch, J.A. Experimental conditions can obscure the second high-affinity site in LeuT. *Nat. Struct. Mol. Biol.* **2012**, *19*, 207–211. [CrossRef]
22. Quick, M.; Javitch, J.A. Monitoring the function of membrane transport proteins in detergent-solubilized form. *Proc. Natl. Acad. Sci. USA* **2007**, *104*, 3603–3608. [CrossRef]
23. Schneider, D.K.; Shi, W.; Andi, B.; Jakoncic, J.; Gao, Y.; Bhogadi, D.K.; Myers, S.F.; Martins, B.; Skinner, J.M.; Aishima, J.; et al. FMX-The Frontier Microfocusing Macromolecular Crystallography Beamline at the National Synchrotron Light Source II. *J. Synchrotron. Radiat.* **2021**, *28 Pt 2*, 650–665. [CrossRef] [PubMed]
24. Waterman, D.G.; Winter, G.; Gildea, R.J.; Parkhurst, J.M.; Brewster, A.S.; Sauter, N.K.; Evans, G. Diffraction-geometry refinement in the DIALS framework. *Acta Crystallogr D Struct Biol.* **2016**, *72 Pt 4*, 558–575. [CrossRef] [PubMed]
25. Brewster, A.S.; Waterman, D.G.; Parkhurst, J.M.; Gildea, R.J.; Young, I.D.; O'Riordan, L.J.; Yano, J.; Winter, G.; Evans, G.; Sauter, N.K. Improving signal strength in serial crystallography with DIALS geometry refinement. *Acta Crystallogr D Struct Biol.* **2018**, *74 Pt 9*, 877894. [CrossRef] [PubMed]
26. Evans, P.R. An introduction to data reduction: Space-group determination, scaling and intensity statistics. *Acta Cryst. D Biol Cryst.* **2011**, *67 Pt 4*, 282–292. [CrossRef] [PubMed]
27. Evans, P.R.; Murshudov, G.N. How good are my data and what is the resolution? *Acta Cryst. D Biol Cryst.* **2013**, *69 Pt 7*, 1204–1214. [CrossRef]
28. Liu, Q.; Dahmane, T.; Zhang, Z.; Assur, Z.; Brasch, J.; Shapiro, L.; Mancia, F.; Hendrickson, W.A. Structures from anomalous diffraction of native biological macromolecules. *Science* **2012**, *336*, 1033–1037. [CrossRef]
29. Read, R.J.; McCoy, A.J. Using SAD data in Phaser. *Acta Cryst. D Biol Cryst.* **2011**, *67 Pt 4*, 338–344. [CrossRef]
30. Quick, M.; Winther, A.M.; Shi, L.; Nissen, P.; Weinstein, H.; Javitch, J.A. Binding of an octylglucoside detergent molecule in the second substrate (S2) site of LeuT establishes an inhibitor-bound conformation. *Proc. Natl. Acad. Sci. USA* **2009**, *106*, 5563–5568. [CrossRef]
31. Casanal, A.; Lohkamp, B.; Emsley, P. Current developments in Coot for macromolecular model building of Electron Cryo-microscopy and Crystallographic Data. *Protein Sci.* **2020**, *29*, 1069–1078. [CrossRef]
32. Afonine, P.V.; Grosse-Kunstleve, R.W.; Echols, N.; Headd, J.J.; Moriarty, N.W.; Mustyakimov, M.; Terwilliger, T.C.; Urzhumtsev, A.; Zwart, P.H.; Adams, P.D. Towards automated crystallographic structure refinement with phenix.refine. *Acta Cryst. D Biol Cryst.* **2012**, *68 Pt 4*, 352–367. [CrossRef] [PubMed]
33. Thorn, A.; Sheldrick, G.M. ANODE: Anomalous and heavy-atom density calculation. *J. Appl. Crystallogr.* **2011**, *44 Pt 6*, 1285–1287. [CrossRef] [PubMed]
34. Williams, C.J.; Headd, J.J.; Moriarty, N.W.; Prisant, M.G.; Videau, L.L.; Deis, L.N.; Verma, V.; Keedy, D.A.; Hintze, B.J.; Chen, V.B.; et al. MolProbity: More and better reference data for improved all-atom structure validation. *Protein. Sci.* **2018**, *27*, 293–315. [CrossRef] [PubMed]
35. Aurelius, O.; Duman, R.; El Omari, K.; Mykhaylyk, V.; Wagner, A. Long-wavelength macromolecular crystallography-First successful native SAD experiment close to the sulfur edge. *Nucl. Instrum. Methods Phys. Res. B* **2017**, *411*, 12–16. [CrossRef]
36. Weinert, T.; Olieric, V.; Waltersperger, S.; Panepucci, E.; Chen, L.; Zhang, H.; Zhou, D.; Rose, J.; Ebihara, A.; Kuramitsu, S.; et al. Fast native-SAD phasing for routine macromolecular structure determination. *Nat. Methods* **2015**, *12*, 131–133. [CrossRef] [PubMed]
37. Liebschner, D.; Yamada, Y.; Matsugaki, N.; Senda, M.; Senda, T. On the influence of crystal size and wavelength on native SAD phasing. *Acta Cryst. D Struct Biol.* **2016**, *72 Pt 6*, 728–741. [CrossRef]
38. Noskov, S.Y.; Roux, B. Control of ion selectivity in LeuT: Two Na+ binding sites with two different mechanisms. *J. Mol. Biol.* **2008**, *377*, 804–818. [CrossRef]
39. Ma, J.; Lei, H.T.; Reyes, F.E.; Sanchez-Martinez, S.; Sarhan, M.F.; Hattne, J.; Gonen, T. Structural basis for substrate binding and specificity of a sodium-alanine symporter AgcS. *Proc. Natl. Acad. Sci. USA* **2019**, *116*, 2086–2090. [CrossRef]
40. Shaffer, P.L.; Goehring, A.; Shankaranarayanan, A.; Gouaux, E. Structure and mechanism of a Na+-independent amino acid transporter. *Science* **2009**, *325*, 1010–1014. [CrossRef]
41. Errasti-Murugarren, E.; Fort, J.; Bartoccioni, P.; Diaz, L.; Pardon, E.; Carpena, X.; Espino-Guarch, M.; Zorzano, A.; Ziegler, C.; Steyaert, J.; et al. L amino acid transporter structure and molecular bases for the asymmetry of substrate interaction. *Nat. Commun.* **2019**, *10*, 1807. [CrossRef] [PubMed]
42. Jungnickel, K.E.J.; Parker, J.L.; Newstead, S. Structural basis for amino acid transport by the CAT family of SLC7 transporters. *Nat. Commun.* **2018**, *9*, 550. [CrossRef] [PubMed]

43. Tang, L.; Bai, L.; Wang, W.H.; Jiang, T. Crystal structure of the carnitine transporter and insights into the antiport mechanism. *Nat. Struct Mol. Biol.* **2010**, *17*, 492–496. [CrossRef]
44. Kazmier, K.; Claxton, D.P.; McHaourab, H.S. Alternating access mechanisms of LeuT-fold transporters: Trailblazing towards the promised energy landscapes. *Curr. Opin. Struct Biol.* **2017**, *45*, 100–108. [CrossRef] [PubMed]
45. Krishnamurthy, H.; Gouaux, E. X-ray structures of LeuT in substrate-free outward-open and apo inward-open states. *Nature* **2012**, *481*, 469–474. [CrossRef]
46. Malinauskaite, L.; Said, S.; Sahin, C.; Grouleff, J.; Shahsavar, A.; Bjerregaard, H.; Noer, P.; Severinsen, K.; Boesen, T.; Schiott, B.; et al. A conserved leucine occupies the empty substrate site of LeuT in the Na(+)-free return state. *Nat. Commun.* **2016**, *7*, 11673. [CrossRef]
47. Christensen, J.J.; Hill, J.O.; Izatt, R.M. Ion binding by synthetic macrocyclic compounds. *Science* **1971**, *174*, 459–467. [CrossRef]
48. Hendrickson, W.A. Anomalous diffraction in crystallographic phase evaluation. *Q Rev. Biophys.* **2014**, *47*, 49–93. [CrossRef]
49. Kawakami, K.; Umena, Y.; Kamiya, N.; Shen, J.R. Location of chloride and its possible functions in oxygen-evolving photosystem II revealed by X-ray crystallography. *Proc. Natl. Acad. Sci. USA* **2009**, *106*, 8567–8572. [CrossRef]
50. Zhou, Y.; MacKinnon, R. The occupancy of ions in the K+ selectivity filter: Charge balance and coupling of ion binding to a protein conformational change underlie high conduction rates. *J. Mol. Biol.* **2003**, *333*, 965–975. [CrossRef]
51. Kazantsev, A.V.; Krivenko, A.A.; Pace, N.R. Mapping metal-binding sites in the catalytic domain of bacterial RNase P RNA. *RNA* **2009**, *15*, 266–276. [CrossRef] [PubMed]
52. Langan, P.S.; Vandavasi, V.G.; Weiss, K.L.; Afonine, P.V.; El Omari, K.; Duman, R.; Wagner, A.; Coates, L. Anomalous X-ray diffraction studies of ion transport in K(+) channels. *Nat. Commun.* **2018**, *9*, 4540. [CrossRef] [PubMed]

Disclaimer/Publisher's Note: The statements, opinions and data contained in all publications are solely those of the individual author(s) and contributor(s) and not of MDPI and/or the editor(s). MDPI and/or the editor(s) disclaim responsibility for any injury to people or property resulting from any ideas, methods, instructions or products referred to in the content.